

## Article

# Research on the Damage Model of Cold Recycled Mixtures with Asphalt Emulsion under Freeze-Thaw Cycles

Ye Yang<sup>1,2</sup>, Zongguang Sun<sup>1</sup>, Yanhai Yang<sup>2,\*</sup>, Chonghua Wang<sup>2</sup> and Lin Qi<sup>3,\*</sup>

<sup>1</sup> College of Transportation Engineering, Dalian Maritime University, Dalian 116026, China; yangye@sjzu.edu.cn (Y.Y.); sun@dmlu.edu.cn (Z.S.)

<sup>2</sup> School of Transportation and Geomatics Engineering, Shenyang Jianzhu University, Shenyang 110168, China; chonghw@126.com

<sup>3</sup> School of Civil Engineering, Shenyang Urban Construction University, Shenyang 110167, China

\* Correspondence: yhyang@sjzu.edu.cn (Y.Y.); qilin6126@126.com (L.Q.)

**Abstract:** Cold recycled mixtures with asphalt emulsion (CRME) suffer the majority of damage from freezing and thawing cycles in seasonal freezing regions. However, an effective model for describing the internal damage evolution behavior of the CRME is still lacking. The objective of this study is to explore the performance of the destroy and damage model of the CRME subjected to freezing and thawing cycles with various water contents. The damage degree of performance at 60 °C and −10 °C, as well as the mechanical properties, were first analyzed in the laboratory. Then, the damage evolution models were established based on macroscopic properties, reliability, and damage theory. The results showed that the performance of the CRME decreased obviously as the number of freezing and thawing cycles increased; after 20 freezing and thawing cycles, the damage degree of 60 °C shear strength and 15 °C and −10 °C indirect tensile strength were 21.5%, 20.6%, and 19.8% at dry condition, but they were 34.9%, 31.8%, and 44.8% at half water saturation condition and 51.5%, 49.1%, and 56.1% at complete water saturation condition; the existence of water and the phase transition of water changed the failure characteristics of the CRME; the correlation coefficient of the damage model parameters was more than 0.98, so the damage evolution model could reveal the internal damage evolution law. Clearly, the freezing and thawing cycles accelerated the damage caused by CRME.

**Keywords:** asphalt emulsion; cold recycled mixtures; damage model; freezing and thawing cycles; property destroy



**Citation:** Yang, Y.; Sun, Z.; Yang, Y.; Wang, C.; Qi, L. Research on the Damage Model of Cold Recycled Mixtures with Asphalt Emulsion under Freeze-Thaw Cycles. *Processes* **2023**, *11*, 3031. <https://doi.org/10.3390/pr11103031>

Academic Editors: Dicho Stratiev, Dobromir Yordanov, Aijun Guo and Amir Tabakovic

Received: 31 August 2023  
Revised: 13 October 2023  
Accepted: 19 October 2023  
Published: 21 October 2023



**Copyright:** © 2023 by the authors. Licensee MDPI, Basel, Switzerland. This article is an open access article distributed under the terms and conditions of the Creative Commons Attribution (CC BY) license (<https://creativecommons.org/licenses/by/4.0/>).

## 1. Introduction

With increasing of the road service life, an increasing number of early-built roads require annual maintenance, causing a dramatic enhancement in the amount of old asphalt material [1]. The disposal of old asphalt materials demands a large amount of land and pollutes the environment [2]. The topic of resource conservation and environmental friendliness has gradually risen to prominence in road construction. Asphalt pavement recycling has become an excellent technique in road construction and maintenance [3,4]. Due to the depression of aggregate, cost, and carbon emissions, cold recycling technology has been widely accepted globally and adopted in many countries [5–7].

Zhang J et al. [8] studied the influences of compaction and water contents on the properties of the CRME, and a design approach for CRME using single compaction was presented. Han Z et al. [9] demonstrated that the vertical vibration testing method showed more excellent mechanical and fatigue performances than Marshall compaction and Superpave Gyrotory Compactor on cold recycled mixtures. And the number and diameter of voids and fractal dimension of the vertical vibration testing method samples were similar to actual core samples in the vertical direction. Chen T et al. [10] proposed that cement and asphalt emulsion need to be completely mixed before the mixing between aggregate and mortar to achieve the more excellent property of the cold recycled mixture; moreover,

aggregate stirred with asphalt emulsion firstly may be an excellent design. Gao L et al. [11] showed that the cold in-place recycling mixtures tend to have larger size and a lower amount of air voids. Kim Y et al. [12] stated that emulsion form and residual asphalt stiffness of reclaimed asphalt pavement (RAP) materials had impacted on the dynamic modulus, flow number, and flow time. Jiang J et al. [13] obtained that the polymer modifiers could enhance the high-temperature property obviously, and adding chloroprene rubber latex seemed to be a more excellent idea to enhance the high-temperature stability of asphalt emulsion. Zhang J et al. [14] found that a recycling agent had an impact on the fracture energy indicator of more than 60%. Yan J et al. [15] proposed cement had active influences on early-age strength and long-term property of cold recycled mixtures. Yang Y et al. [16] showed cold recycled mixtures had more excellent low-temperature property when adding cement was between 1% and 2%. Dong S et al. [17] concluded the rejuvenation agent, styrene–butadiene rubber latex, and Buton rock asphalt could enhance the comprehensive property of the modified CRME. Moreover, the rejuvenation agent had the largest influence. Du S [18] found polyester fiber, polypropylene fiber, polyacrylonitrile fiber, lignin fiber, and basalt fiber could improve the performance of the emulsion recycled mixture. Polyester fiber had better advancement on fatigue life than others. Xu S et al. [19] found the new cold-mix SBS modified emulsified asphalt had better mechanical performance, rutting performance, and water stability than the normal hot and warm mix asphalt mixtures. In comparison with deicing agents containing calcium chloride, the deicing agents containing calcium magnesium acetate obviously could reduce the disruptive influences of freeze–thaw cycles on the mechanical performance of cold recycled mixtures using polymer-modified bitumen emulsion [20]. Yang Y et al. [21] discovered the numerical value and quantity of the tensile force chain in DEM raised markedly; as the stress ratio increased, the fatigue performance decreased significantly. Lin J et al. [22] presented the viscoelastic of the CRME was worse than HMA. The fatigue life of the CRME was 10%–20% normal asphalt mixture at high strain. Xia Y et al. [6] proposed the initial cracking point appeared at approximately 60% of the fatigue life based on the SCB fatigue test through image analysis. The value of the destroyed variable was 0.06–0.17 at the initial cracking point according to the cracking model.

However, the road performance of the CRME decayed obviously, and diseases such as crushing and loosening appeared in the seasonal frozen region [23]. Water was the key factor for the destruction. Due to temperature variation, the water would freeze and thaw with the changing seasons, causing significant damage to the CRME [24]. Lachance-Tremblay et al. [25] demonstrated the linear viscoelastic properties containing glass aggregates were significantly altered during freezing and thawing cycles. The addition of hydrated lime containing glass aggregates obviously decreased the linear viscoelastic property. Freezing and thawing cycles enhanced the interior destruction of the asphalt mixture, resulting in air voids increasing and adhesion decreasing [26]. Fan Z et al. [27] observed that the fatigue life of asphalt mixtures reduced with saturation and freezing–thawing cycles increasing. Fu L. et al. [28] showed that freezing and thawing cycles changed the failure type of asphalt mixtures, made it harder for microcracks to form early on, sped up the growth of macrocracks, and made it easier for asphalt and aggregates to separate. Wang T. et al. [29] found the tensile modulus of steel slag, basalt, and recycled aggregate permeable asphalt concrete decreased by 80–90% after 20 freezing–thawing cycles. Ud Din et al. [30] found freezing and thawing could obviously impact the compressive strength, air voids, fatigue cracking, and the rutting of the asphalt pavement. Fatigue and rutting were more sensitive to climatic conditions. Xu H et al. [31] presented the interior void evolution law: expansion of original voids; connection of independent voids; occurrence of new voids, demonstrating the nonnegligible impact of pore structure on dynamic flow law subjected to freezing and thawing cycles [32]. Wang J et al. [33] put forward the damage mechanism of the biobased cold-mix epoxy asphalt subjected to freezing and thawing cycles: post-curing and damage of the cross-linking network; agglomeration and aging of asphalt; diffusion and reaction of water. Jin D et al. [34] found asphalt emulsion chip

seal showed a decrease in interlayer shear strength and interlayer tensile strength under repeated loading, freezing, and thawing cycles. The weak bond between asphalt emulsion and aggregate could be due to repeated loading and freezing and thawing behaviors. Zhao H et al. [35] found the indirect tensile strength, the modulus, and the fracture properties of cold recycled mixtures using foamed asphalt significantly decreased subjected to freezing and thawing cycles. Löqvist L et al. [36] presented a new thermodynamics-based multi-scale model of freezing and thawing destruction in asphalt mixtures, which also calculated the destruction from water and traffic. Chen Y et al. [37] presented the freeze–thaw cycles made the nonlinear characteristics of the stress–strain relationship of the asphalt mixture remarkable. Yang Y. et al. [38] concluded the void ratio of CRME went up by 1.06%, the ultrasonic wave velocity and high and low temperature performance all went down, and the splitting strength went down by 26.3% after 20 unsatisfied freezing–thawing cycles. Under freezing and thawing cycles, the voids of vacuum-saturated samples were primarily characterized by the formation of new voids, void expansion, and void bonding [39].

In summary, researchers have conducted a large number of studies on mix design, air void characteristics, performance evaluation, early strength, additives, and fatigue performance to improve the CRME. Although extensive research has been conducted on normal asphalt mixtures during freezing and thawing cycles, a few studies have been conducted on the CRME, despite the fact that its application in a seasonally frozen area is crucial. CRME has greater air voids (8–13%) than normal asphalt mixture. The water could easily permeate the CRME and weaken the bond among asphalt, old asphalt, new aggregate, and old aggregate. The adhesion has an immediate impact on the performance of the CRME. Therefore, the aim of this research is to explore the performance degradation and damage model of the CRME under freezing and thawing cycles with various water contents. The uniaxial penetration test and indirect tensile test are carried out to evaluate the high–low temperature performance and mechanical properties. The damage degree of the 60 °C shear strength and 15 °C and –10 °C indirect tensile strength are calculated and analyzed. Finally, the damage model of CRME is developed to reveal the internal law of damage evolution based on macroscopic properties, reliability, and damage theory.

## 2. Materials and Methods

### 2.1. Materials

Table 1 illustrates the characteristics of asphalt emulsion referencing JTG T5521-2019 [40]. The RAP was milled from a first-class highway in Shenyang, China and divided into 0 mm, 0.075 mm, 0.15 mm, 0.3 mm, 0.6 mm, 1.18 mm, 2.36 mm, 4.75 mm, 9.5 mm, 13.2 mm, 16 mm, and finally 19 mm. Referring to JTG T5521-2019 [40], the sand equivalent value of RAP was 65%, which met the specification requirements that is not less than 50%. The characteristics of the new aggregate satisfied the requirement of the JTG F40-2004 [41], which was divided into the single size. The biggest size of RAP could not satisfy the gradation composition of CRME referencing to JTG T5521-2019 in China [40]. A total of 19–26.5 mm of new aggregate was added. Drinking water and 32.5# of regular Portland cement were added in the meantime.

**Table 1.** Characteristics of asphalt emulsion [24].

Characteristic	Requirements	Results
Demulsification speed	Slow-cracking	Slow-cracking
Particle charge	Cation (+)	Cation (+)
Remained content on 1.18 mm/wt%	≤0.1	0.021
Solid content/wt%	>60	63.6
Penetration (25 °C, 100 g, 5 s)/0.1 mm	50–130	69.5
Softening point/°C	—	45.6
Ductility (15 °C)/cm	≥40	76.5
Solubility in trichloroethylene/wt%	≥97.5	99.1

**Table 1.** Cont.

Characteristic	Requirements	Results
Storage stability at 1 d/wt%	$\leq 1$	0.4
Storage stability at 5 d/wt%	$\leq 5$	2.6

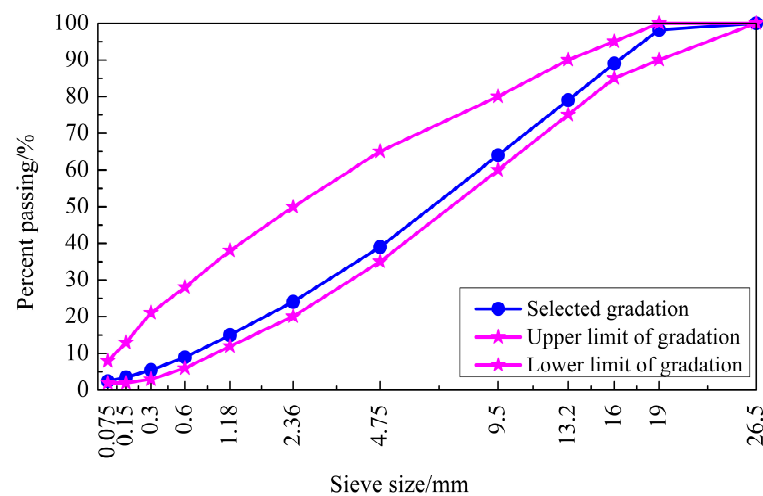
## 2.2. Mixture Design and Preparation of the Samples

### 2.2.1. Mixture Design

The selected gradation and composition of RAP and new aggregate are displayed in Table 2 [16]. The cement dosage was adopted by the early result, which was 1.5 wt% [16]. The selected gradation of the CRME is shown in Figure 1. The optimum water content of CRME was determined referencing JTG E40-2007 [42], which was 3.0 wt%. The optimum asphalt emulsion content of CRME was determined referencing to JTG T5521-2019 [40], which was 3.5 wt%.

**Table 2.** Selected gradation of RAP and new aggregates.

Size/mm	26.5	19	16	13.2	9.5	4.75	2.36	1.18	0.6	0.3	0.15	0.075
Passing rate/% RAP (68.95%)	100	100	88.8	78.7	63.5	38.1	22.8	13.7	7.6	4.1	2.0	1.0
Passing rate/% New Aggregate (29.55%)	100	93.9	88.8	78.7	63.5	38.1	22.8	13.7	7.6	4.1	2.0	1.0

**Figure 1.** Selected gradation of CRME.

### 2.2.2. Preparation of the Samples

The Superpave gyratory compactor (AFG2C) was applied to form the samples. The 1.25° rotation compaction angle, 600 kPa vertical compressive stress, and 30 rpm were set in a Superpave gyratory compactor. The diameter of the sample was  $100 \pm 0.5$  mm. The CRME samples were molded under the optimum mixture composition. Firstly, the mixture was placed into the mold and compacted up to 63.5 mm in height. Then, all the samples were cured in a 60 °C environmental oven for more than 40 h. Finally, the samples were put in an indoor temperature environment for longer than 12 h [40].

## 2.3. Experimental Methods

### 2.3.1. Freezing and Thawing Test

The cured sample was subjected to a freezing and thawing test with various water content. The dry condition, half water saturation condition, and complete water saturation condition were adopted. The parallel four samples were carried out for every test under a saturated condition and different freezing and thawing cycles.

- (1) Dry condition, namely 0% water saturation condition. The cured samples were directly covered with plastic preservative film.
- (2) Complete water saturation condition, namely 100% water saturation condition. Firstly, the cured samples were vacuumed for 15 min in water. The vacuum pressure was 98.3~98.7 kPa. Secondly, the vacuumed samples were kept in normal pressure water for longer than 2 h until absorbing water completely. Thirdly, the surface of vacuum saturated samples was dried through the wet cloth and covered with plastic preservative film.
- (3) Half water-saturation condition, namely 50% water saturation condition. The cured samples were weighed. The weighted samples were vacuum saturated according to (2). The weight of the vacuum-saturated sample was measured. The environmental furnace then reduced the weight of water absorption by half. Finally, the surface of the half water-saturated specimens was covered with plastic preservative film and placed in an indoor environment for more than 12 h.

The samples with different water contents were frozen and thawed. The sample was stored at  $-20\text{ }^{\circ}\text{C}$  and  $20\text{ }^{\circ}\text{C}$  for 6 h, respectively, completing one freeze-thaw cycle. The whole samples were frozen-thawed zero, five, ten, fifteen, and twenty times, respectively [27,43]. The frozen-thawed samples were used to evaluate the characteristics of CRME after drying. The partial samples are shown in Figure 2.



**Figure 2.** The partial samples before experiment.

### 2.3.2. Uniaxial Penetration Test

The uniaxial penetration test was used to evaluate the high-temperature performance of CRME at  $60 \pm 1\text{ }^{\circ}\text{C}$ . The 1 mm per minute was used as the loading rate referencing JTG D50-2017 [44]. The electromechanical universal tester (70-S18B2) (Controls S.R.L., Milan, Italy) was used for the test to obtain the maximum load. The shear strength was obtained by Equation (1).

$$R_S = f \times P/A \quad (1)$$

where  $R_S$ ,  $f$ ,  $P$ , and  $A$  represent the shear strength (MPa), the sample dimension correction coefficient  $f = 0.34$ , the maximum loading (N), and the cross-sectional area ( $\text{mm}^2$ ), respectively.

### 2.3.3. Indirect Tensile Test

The indirect tensile test was performed at  $15 \pm 0.5\text{ }^{\circ}\text{C}$  based on the loading rate of 50 mm per minute to evaluate the mechanical property referencing JTG E20-2011 [45].

However, the indirect tensile test was performed at  $-10 \pm 0.5$  °C based on the loading rate of 1 mm per minute to reveal the low-temperature cracking resistance referencing JTG E20-2011 [45]. The electromechanical universal tester (70-S18B2) (Controls S.R.L., Milan, Italy) was used for the indirect tensile test to obtain the limit load. The indirect tensile strength was obtained by Equation (2).

$$R_T = 0.006287F/h \quad (2)$$

where  $R_T$ ,  $F$ , and  $h$  represent the indirect tensile strength (MPa), the limit loading (N), and the height of the sample (mm), respectively.

## 2.4. Modeling Method

### 2.4.1. Basic Model Assumptions

If the CRME could satisfy the basic assumptions of the general model of reliability and damage theory, the damage evolution law of CRME could be analyzed under freezing–thawing cycles [46,47]. The modelling of each surface of the cube subjected to the same damage was adopted to investigate the damage situation of CRME under freezing and thawing cycles with various water contents.

Situation 1: The interior of CRME was considered continuous and homogeneous. RAP, new aggregate, cement, and asphalt emulsion conform to the random distribution and were proportionally smaller than the sample. Consequently, the sample could be considered as homogenous material.

Situation 2: The boundary of the CRME was in the same freezing and thawing conditions. The damage was developed from outside to inside gradually under freeze–thaw cycles with various water content. Therefore, all microscopic unit points with the shortest distance between the interior and boundary of CRME satisfied the damage evolution law. Each surface of the cube subjected to the same damage was drawn in Figure 3.

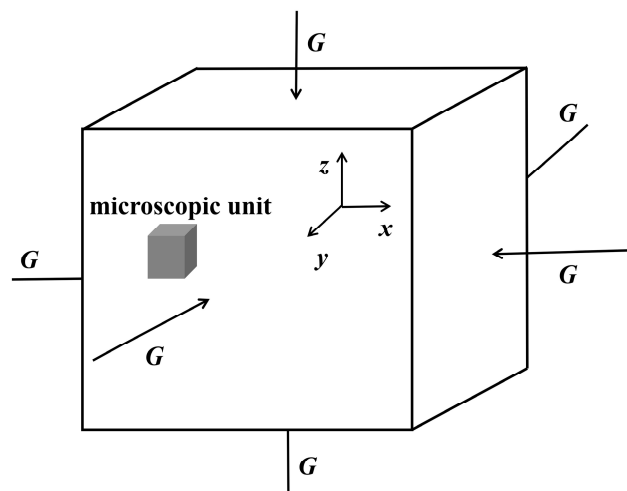


**Figure 3.** Each surface of the cube suffers the same amount of damage.

Situation 3: The destroyed occurrence of CRME was from the gradually accumulated interior damage as freezing and thawing cycles increased. The failure possibility of every component increased over time in CRME exposed to freezing and thawing cycles with various water contents. Therefore, it was considered that the destruction of CRME accorded to the Weibull damage distribution under freezing and thawing cycles, as represented by Equation (3).

$$F(t) = 1 - \exp [-(\lambda t)^\alpha] \quad (3)$$

where  $t$ ,  $\lambda$ , and  $\alpha$  represent the number of freezing and thawing cycles (time), the scale factor (dimensionless), and the shape factor (dimensionless), respectively.

Situation 4: Each point was subjected to the same amount of damage. Based on the characteristics of the Weibull distribution, the failure curve shape of each point was the same approximately. Consequently, it was possible to conclude that the shape factor  $\alpha$  was the same. If the microscopic unit point had any coordinate  $(x, y, z)$ , then Equation (4) could be used to determine the shape factor  $\alpha$ .

$$\lambda(x, y, z) = \lambda(|x|, |y|, |z|) \quad (4)$$

#### 2.4.2. Model Derivation

The microscopic unit  $(x, y, z)$  was selected randomly in CRME. The probability density function of the internal point from the microscopic unit was  $f(x, y, z; t)$  at  $t$  time. Therefore, the number of damaged microscopic units was  $V(x, y, z; t)$  at time  $t$ . The random variable satisfied the spatial Poisson distribution requirement. Therefore, Equation (5) represents the probability  $P$  of internal point failure.

$$P = f(x, y, z; t) d\zeta d\eta d\sigma \quad (5)$$

According to the mathematical expectation of the Poisson distribution, the mathematical expectation of  $V(x, y, z; t)$  could be derived as shown in Equation (6).

$$E(V) = nP = dx dy dz d\zeta^{-1} d\eta^{-1} d\sigma^{-1} f(x, y, z; t) d\zeta d\eta d\sigma = f(x, y, z; t) dx dy dz \quad (6)$$

where the  $n$  represents the quantity of sample points in the space area.

The failure volume of the whole section was shown in Equation (7).

$$V = \iint_{V_0} E(V) \quad (7)$$

According to the previous studies [47], the study defined the degree of damage using Equation (8).

$$D = V/V_0 \quad (8)$$

where  $D$ ,  $V$ ,  $V_0$  represent the degree of damage (%), the volume of the damaged unit (dimensionless), and the volume of the original unit (dimensionless), respectively.

According to Equations (3)–(8), the damage degree equation could be obtained as shown in Equation (9).

$$D = V_0^{-1} \iint_{V_0} f(x, y, z; t) dx dy dz = V_0^{-1} \iint_{V_0} \alpha(\lambda t)^{\alpha-1} \exp[-(\lambda t)^\alpha] dx dy dz \quad (9)$$

#### 2.4.3. Numerical Algorithm of Damage Evolution

Equation (9) could be altered through discretization of the calculated spatial region. In the calculated spatial region, each boundary was divided into  $N$  parts on average, and  $N$  was a dual number. Based on situation 2, the  $i$ -layer unit number distribution was identical. According to Equation (10), the units with the shortest distance from the model boundary were determined.

$$N_i = 6N^2 - 24iN + 24i^2 - 12N + 24i + 8 \quad (10)$$

where  $i = 0, 1, 2, \dots, (n = N/2 - 1)$ , respectively.

At  $t$  time, the distribution function of  $i$ -layer unit damage was  $F_i(t)$ . When the number of sample points of the Poisson distribution was large, the Poisson distribution could be transformed into the Bernoulli distribution based on the relationship between the Poisson distribution and the Bernoulli distribution, namely  $N_i$  damage in the unit of the  $i$  layer. The mathematical expectation of the event  $\Phi_i$  was shown in Equation (11).

$$E(\Phi_i) = N_i F_i(t) \quad (11)$$

Based on situation 3, Equation (12) could be obtained.

$$F_i(t) = 1 - \exp [-(\lambda t)^\alpha] \quad (12)$$

The scale factor  $\lambda_i$  was simulated with the linear formula, and the mesh was sufficiently divided. The influence of micro-unit size could be neglected. The scale factor  $\lambda_i$  could be shown in Equation (13).

$$\lambda_i = \lambda_0 - 2iv / (N - 2) \quad (13)$$

where  $\lambda$  and  $v$  represent the scale factor (dimensionless) and the gradient factor (dimensionless),  $i = 0, 1, 2, \dots, (n = N/2 - 1)$ , respectively.

The microscopic unit was in the outer layer at  $i = 0$ , and  $\lambda_i = \lambda_0$ . The microscopic unit was in the inner layer at  $i = N/2 - 1$ , and  $\lambda_i = \lambda_0 - v$ . The average scale factor of the outer and inner layers of the CRME could be substituted into the calculation. The mathematic expectation of the unit damage event  $\omega$  at time  $t$  could be obtained as shown in Equation (14).

$$E(\omega) = \sum_{i=0}^{N/2-1} E(\phi_i) = \sum_{i=0}^{N/2-1} N_i F_i(t) \quad (14)$$

According to the Equation (14), the expected value of regional damage degree could be calculated. As shown in Equation (15).

$$E(D) = E(\omega)/V_0 = N^{-3} \sum_{i=0}^{N/2-1} \left( 6N^2 - 24iN + 24i + 8 \right) \times \left\{ 1 - \exp \left[ - \left( \lambda_0 t - \frac{ivt}{N/2-1} \right)^\alpha \right] \right\} \quad (15)$$

$E(D) = 0$  at  $t = 0$ , which showed that the damage degree of CRME was 0 without freezing and thawing cycles.  $E(D) = 1$  at  $t \rightarrow \infty$ , which showed that the damage degree of CRME was 1 after infinite freezing and thawing cycles. Based on the application of the equal strain assumption in macroscopic phenomenological damage mechanics, the damage degree of the CRME after freezing and thawing cycles could be calculated according to Equation (16).

$$D_n = (E_0 - E_n)/E_0 \quad (16)$$

where  $D_n$ ,  $E_0$ , and  $E_n$  represent the degree of damage of CRME after  $n$  freezing and thawing cycles, the performance of the CRME without freezing and thawing cycles, and the performance of CRME after  $n$  freezing and thawing cycles, respectively.

### 3. Results and Discussions

#### 3.1. Experimental Results

The results of the 60 °C uniaxial penetration test and 15 °C, and −10 °C indirect tensile strength test under freezing and thawing cycles with various water contents are shown in Table 3.

#### 3.2. Damage Models

The damage models of the high–low temperature performance and mechanical property of the CRME were used to investigate the damage situation. The damage degree of CRME was calculated based on the Equation (16). The damage degree results of CRME are displayed in Table 4. Figure 4 illustrates the damage degree change trend of CRME under freezing and thawing cycles with various water content.

**Table 3.** Test results of CRME under freezing and thawing cycles with various water contents.

Freeze-Thaw Cycles/Times	60 °C Shear Strength/MPa			15 °C Indirect Tensile Strength/MPa			−10 °C Indirect Tensile Strength/MPa		
	Dry Condition	Half Water Saturation Condition	Complete Water Saturation Condition	Dry Condition	Half Water Saturation Condition	Complete Water Saturation Condition	Dry Condition	Half Water Saturation Condition	Complete Water Saturation Condition
0	0.573 (0.041)	0.548 (0.040)	0.556 (0.039)	0.65 (0.023)	0.63 (0.015)	0.66 (0.003)	1.11 (0.008)	1.05 (0.012)	1.07 (0.019)
5	0.542 (0.024)	0.483 (0.033)	0.459 (0.057)	0.60 (0.016)	0.56 (0.011)	0.55 (0.003)	1.03 (0.023)	0.90 (0.018)	0.86 (0.010)
10	0.491 (0.015)	0.431 (0.018)	0.374 (0.020)	0.57 (0.011)	0.49 (0.007)	0.46 (0.008)	0.96 (0.031)	0.77 (0.026)	0.70 (0.009)
15	0.468 (0.029)	0.396 (0.022)	0.317 (0.012)	0.54 (0.005)	0.44 (0.012)	0.38 (0.007)	0.92 (0.014)	0.65 (0.009)	0.55 (0.011)
20	0.455 (0.038)	0.374 (0.031)	0.283 (0.019)	0.51 (0.017)	0.41 (0.006)	0.32 (0.008)	0.86 (0.014)	0.58 (0.006)	0.47 (0.007)

The data of () are the standard deviation.

**Table 4.** The damage degree results of CRME under freezing and thawing cycles with various water content.

Freeze-Thaw Cycles/Times	Damage Degree of 60 °C Shear Strength/%			Damage Degree of 15 °C Indirect Tensile Strength/%			Damage Degree of −10 °C Indirect Tensile Strength/%		
	Dry Condition	Half Water Saturation Condition	Complete Water Saturation Condition	Dry Condition	Half Water Saturation Condition	Complete Water Saturation Condition	Dry Condition	Half Water Saturation Condition	Complete Water Saturation Condition
0	0	0	0	0	0	0	0	0	0
5	7.7	11.1	16.7	5.4	11.9	17.4	7.2	14.3	19.6
10	12.3	22.2	30.3	14.3	21.4	32.7	13.5	26.7	34.6
15	16.9	30.2	42.4	18.3	27.7	43.0	17.1	38.1	48.6
20	21.5	34.9	51.5	20.6	31.8	49.1	19.8	44.8	56.1

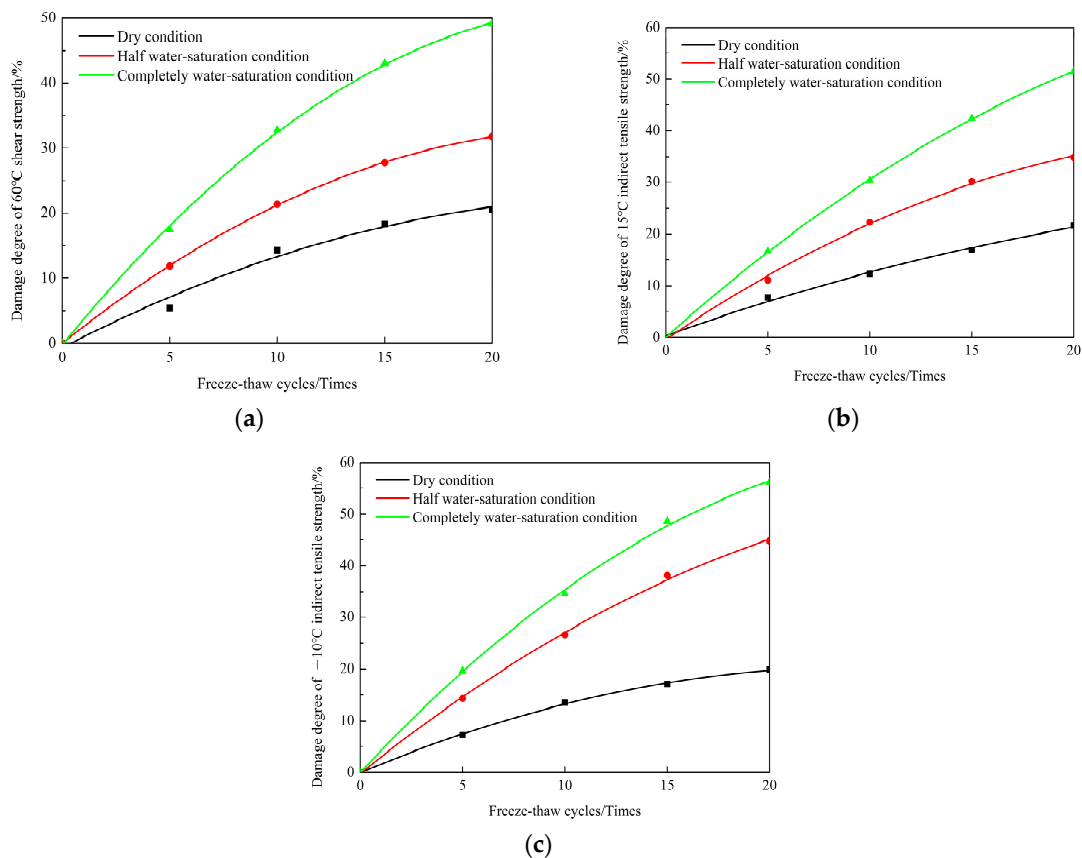


**Figure 4.** Damage degree change trend under freezing–thawing cycles with various water contents: (a) 60 °C shear strength; (b) 15 °C indirect tensile strength; (c) −10 °C indirect tensile strength.

As shown in Table 4 and Figure 4, with the number of freezing and thawing cycles increasing, the damage degree of the high–low temperature performance and mechanical property of CRME increased. As the saturation rate rises, the performance changes under freezing–thawing cycles become more pronounced. It indicated that the temperature cycle would damage the CRME and that the water would exacerbate the damage of the CRME during the temperature cycle.

Three parameters ( $\alpha$ ,  $\lambda_0$ ,  $v$ ) of the damage evolution model could be achieved by the nonlinear fitting of Equation (15) according to the damage degree of CRME from Table 4. Therefore, the damage evolution model could be established. The calculation results of the parameters would be affected by the number of grids  $N$ . The fitting results would become more accurate as the number of grids  $N$  increased. The parameters of the damage evolution model would also be more accurate. However, the iteration times of the damage evolution model would become higher as the number of grids  $N$  increased, which would affect the computational efficiency. Therefore, it was necessary to determine an appropriate  $N$  value. The MATLAB (2018A) software was used to nonlinearly fit the parameters of the damage evolution model. The initial value of  $N$  was set to 4, and  $N = N + 2$  was used for the cyclic calculation until the parameters were stable. The degree of damage of high–low temperature performance and mechanical property of the CRME and the number of freezing and thawing cycles were fitted with different water contents. The predicted data became stable, and the calculation result was accurate when  $N = 48$ . In order to obtain a stable model and accurate results,  $N = 100$  was adopted for calculation during the study.

### 3.3. Parameter Analysis of Damage Model

The damage evolution models were established based on the damage degree data calculated by different properties under 20 freezing and thawing cycles. The calculated performance parameters are shown in Table 5. The damage degree evolution diagrams of 60 °C shear strength and 15 °C and –10 °C indirect tensile strength are shown in Figures 5–7.

Table 5. Parameters results of damage model.

Performance	Water-Saturated Condition	Correlation Coefficient	Parameters of Damage Model		
			The Shape Factor $\alpha$	The Scale Factor $\lambda$	The Gradient Factor $v$
15 °C indirect tensile strength	Dry condition	0.995	0.7873	0.0208	0.0197
	Half water saturation condition	0.997	1.0427	0.0455	0.0451
	Complete water saturation condition	0.996	1.3223	0.0838	0.0831
60 °C shear strength	Dry condition	0.985	0.7821	0.0252	0.0218
	Half water saturation condition	0.998	0.9898	0.0488	0.0466
	Complete water saturation condition	0.999	1.2009	0.0875	0.0871
–10 °C indirect tensile strength	Dry condition	0.994	0.9115	0.0265	0.0234
	Half water saturation condition	0.999	1.2011	0.0675	0.0668
	Complete water saturation condition	0.988	1.4273	0.1046	0.0988

Table 5 showed that the damage evolution model of CRME fit well and that the correlation coefficients were greater than 0.98 when freezing and thawing cycles happened. The shape factor, scale factor, and gradient factor showed different characteristics of the CRME under freezing and thawing cycles with different water contents. Figures 5–7 showed that the model fitting effect was good and the error was small.

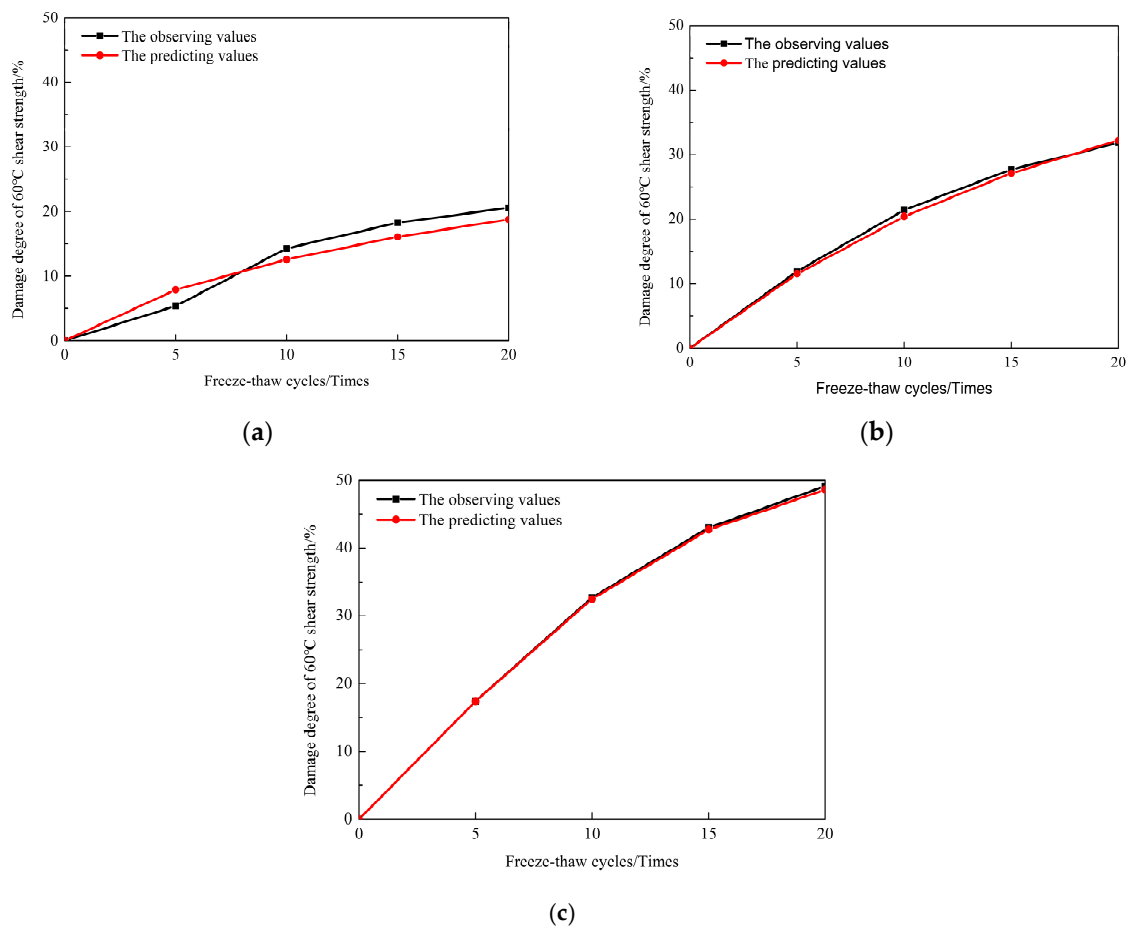


**Figure 5.** Damage degree evolution diagram of 60 °C shear strength: (a) dry condition; (b) half water saturation condition; (c) complete water saturation condition.

The shape factor revealed the failure characteristics of the inner points of the CRME under freezing and thawing cycles with different water contents [47]. Table 5 showed that the shape factors of 60 °C shear strength and 15 °C and −10 °C indirect tensile strength increased from 0.7873 to 1.3223, 0.7821 to 1.2009, 0.9115 to 1.4273, respectively. The shape factors of the CRME were similar to hot asphalt mixtures [46,47]. It indicated the inner points failure of the CRME gradually accumulated with the increasing of water contents. The presence of water and the phase transition of water changed the internal failure characteristics of the CRME [24,39]. The shape factors of 60 °C shear strength and 15 °C and −10 °C indirect tensile strength were different at various water contents, which showed that water contents had different influences on the same performance of CRME.

The scale factor indicated the resistance ability of the internal points of the CRME under freezing and thawing cycles with various water contents. The scale factor was mainly determined by air voids, gradation, additives, and so on [47]. The greater the value of the scale factor, the weaker the ability to resist freezing and thawing damage [46]. As shown schematically in Table 5, the scale factors of 60 °C shear strength and 15 °C and −10 °C indirect tensile strength increased from 0.0208 to 0.0838, 0.0252 to 0.0875, 0.0265 to 0.1046, respectively. The scale factors of the CRME were similar to hot asphalt mixtures [46,47]. It indicated that the resistance ability of CRME decreased with the increasing of water contents. Moreover, the −10 °C indirect tensile strength was influenced by water contents obviously. The frost heaving force from the phase transition of water accelerated the formation of new voids and the connection of voids, which resulted in a significant decrease in performance under freezing and thawing cycles with different water contents [39].

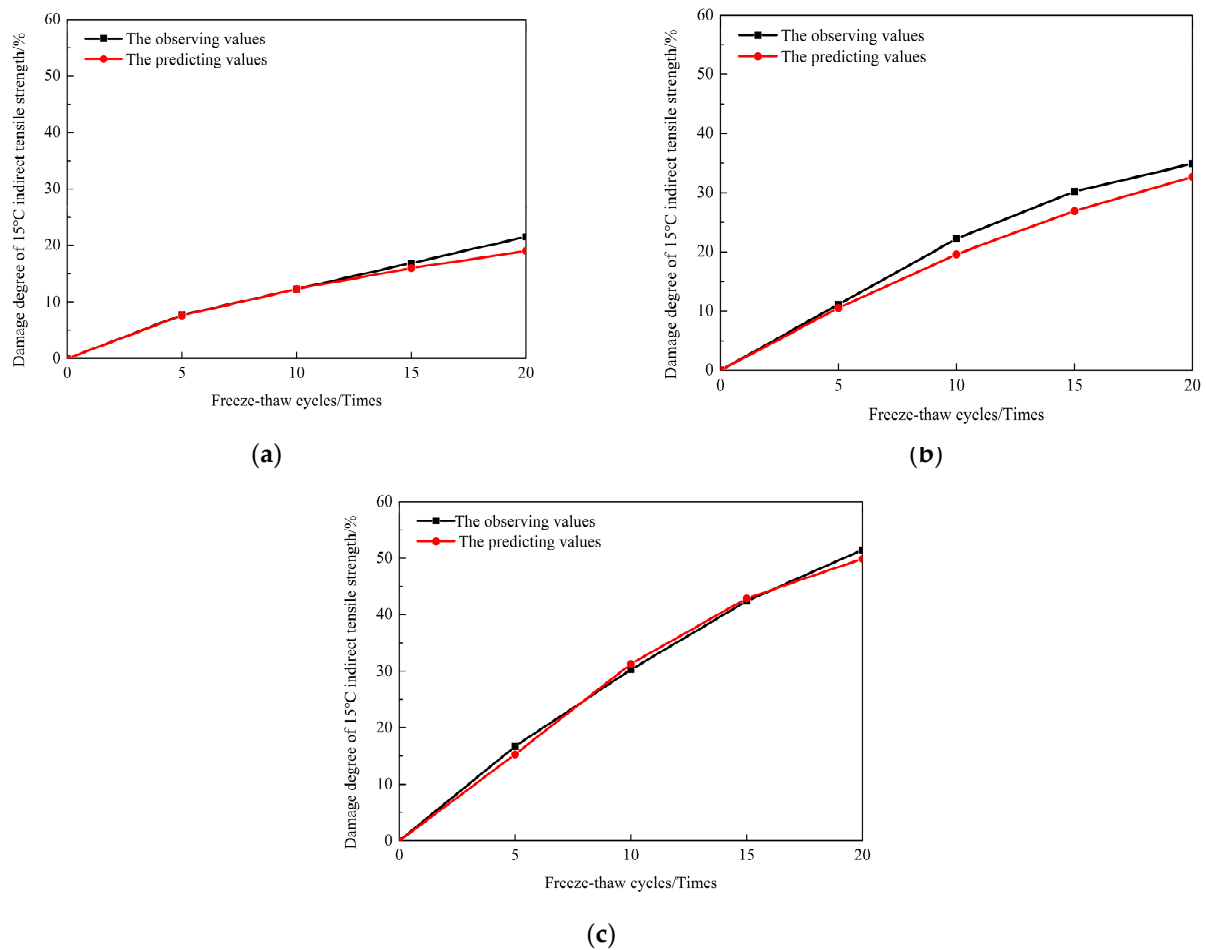


**Figure 6.** Damage degree evolution diagram of 15 °C indirect tensile strength: (a) dry condition; (b) half water saturation condition; (c) complete water saturation condition.

The gradient factor showed the difference in destruction development of the interior points of the CRME under freezing and thawing cycles with different water contents [47]. The absolute value of the gradient factor represented the difference. When the absolute value of the gradient factor was small, the damage to the internal points occurred at the same time, indicating that the material was homogeneous. The gradient factor was positive, which indicated that the damage developed from the surface to the interior. The gradient factor was negative, which indicated that the damage developed from the interior to the surface [46]. The gradient factors of 60 °C shear strength and 15 °C and −10 °C indirect tensile strength increased from 0.0197 to 0.0831, 0.0218 to 0.0871, 0.0234 to 0.0988, respectively. The gradient factor of the CRME was positive, which indicated that the damage developed from the surface to the interior in CRME under freezing and thawing cycles. However, the absolute value of the gradient factor for hot asphalt mixtures was less  $10^{-7}$  [46,47]. It shows that the homogeneity of the CRME was worse than hot mix asphalt. Moreover, the gradient factors of 60 °C shear strength and 15 °C and −10 °C indirect tensile strength increased gradually with the water contents. It indicated the damage of the CRME gradually accumulated with the increasing of water contents.

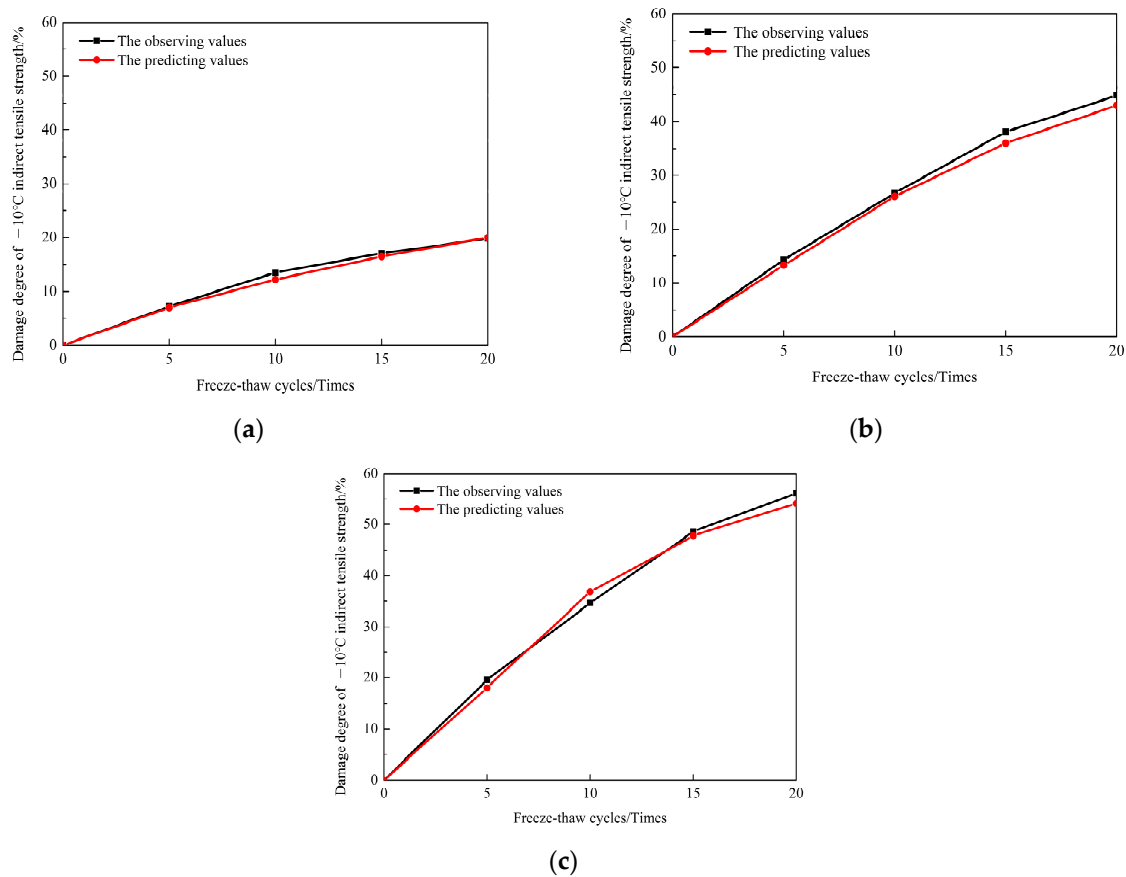


**Figure 7.** Damage degree evolution diagram of  $-10^{\circ}\text{C}$  indirect tensile strength: (a) dry condition; (b) half water saturation condition; (c) completely water saturation condition.

#### 4. Conclusions

In this paper, the damage model investigated the damage characteristics of CRME under freezing–thawing cycles with various water contents. The following conclusions were drawn:

1. The damage degree of  $60^{\circ}\text{C}$  shear strength and  $-10^{\circ}\text{C}$  and  $15^{\circ}\text{C}$  indirect tensile strength of the CRME increases with the freezing and thawing cycles increasing. As the water content increases, the damage degree of performance increases significantly under freezing and thawing cycles.
2. The fitting accuracy of the damage evolution model of CRME was good under freezing and thawing cycles, and the correlation coefficients were greater than 0.98.
3. The shape factor and gradient factor of  $60^{\circ}\text{C}$  shear strength and  $-10^{\circ}\text{C}$  and  $15^{\circ}\text{C}$  indirect tensile strength gradually increased with the increasing degree of saturation. On the contrary, the scale factors gradually decreased with the increase in saturation degree.
4. With the water content increasing, the generation of new voids and the interconnection of voids occurred. The homogeneity of the CRME became worse, resulting in a significant decrease in performance under freezing and thawing cycles with different water contents.
5. Based on the results of the present study and other studies on the CRME subjected to freezing–thawing cycles with various water contents, it is recommended that future studies examine the fatigue performance, dynamic characteristic, and cracking behaviors and establish a multi-scale model to reflect damage mechanisms.

**Author Contributions:** Conceptualization, Y.Y. (Ye Yang) and Z.S.; methodology, Y.Y. (Ye Yang) and L.Q.; software, Y.Y. (Ye Yang) and C.W.; validation, Y.Y. (Ye Yang); formal analysis, Y.Y. (Ye Yang) and L.Q.; investigation, Y.Y. (Yanhai Yang); resources, Y.Y. (Yanhai Yang); data curation, Y.Y. (Ye Yang) and L.Q.; writing—review and editing, Y.Y. (Ye Yang), Z.S., and C.W.; supervision, Y.Y. (Yanhai Yang). All authors have read and agreed to the published version of the manuscript.

**Funding:** This study was supported by the National Natural Science Foundation of China (grant numbers 52278454) and Traffic Science and Technology Project of Liaoning Province, China [grant numbers 202216].

**Data Availability Statement:** Not applicable.

**Acknowledgments:** This research was performed at Dalian Maritime University and Shenyang Jianzhu University.

**Conflicts of Interest:** The authors declare no conflict of interest.

## References

1. Huang, W.; Cao, M.; Xiao, L.; Li, J.; Zhu, M. Experimental study on the fatigue performance of emulsified asphalt cold recycled mixtures. *Constr. Build. Mater.* **2023**, *369*, 130607. [[CrossRef](#)]
2. Ji, J.; Li, J.; Wang, J.; Suo, Z.; Li, H.; Yao, H. Early strength of cold recycled emulsified asphalt mixtures. *J. Mater. Civ. Eng.* **2023**, *35*, 04023088. [[CrossRef](#)]
3. Hu, G.; Yang, Q.; Qiu, X.; Zhang, D.; Zhang, W.; Xiao, S.; Xu, J. Use of DIC and AE for investigating fracture behaviors of cold recycled asphalt emulsion mixtures with 100% RAP. *Constr. Build. Mater.* **2022**, *344*, 128278. [[CrossRef](#)]
4. Han, D.; Liu, G.; Xi, Y.; Zhao, Y. Research on long-term strength formation and performance evolution with curing in cold recycled asphalt mixture. *Case Stud. Constr. Mater.* **2023**, *18*, e01757. [[CrossRef](#)]
5. Zhao, Z.; Ni, F.; Zheng, J.; Cheng, Z.; Xie, S. Evaluation of curing effects on bitumen emulsion-based cold in-place recycling mixture considering field-water evaporation and heat-transfer conditions. *Coatings* **2023**, *13*, 1204. [[CrossRef](#)]
6. Xia, Y.; Lin, J.; Chen, Z.; Cai, J.; Hong, J.; Zhu, X. Fatigue cracking evolution and model of cold recycled asphalt mixtures during different curing times. *Materials* **2022**, *15*, 4476. [[CrossRef](#)]
7. Xiao, F.; Yao, S.; Wang, J.; Li, X.; Amirkhanian, S. A literature review on cold recycling technology of asphalt pavement. *Constr. Build. Mater.* **2018**, *180*, 579–604. [[CrossRef](#)]
8. Zhang, J.; Zheng, M.; Xing, X.; Pei, J.; Zhang, J.; Li, H.; Xu, P.; Wang, D. Investigation on the designing method of asphalt emulsion cold recycled mixture based on one-time compaction. *J. Clean. Prod.* **2021**, *286*, 124958. [[CrossRef](#)]
9. Han, Z.; Liu, Z.; Jiang, Y.; Wu, P.; Li, S.; Sun, G.; Zhang, L. Engineering properties and air void characteristics of cold recycled mixtures with different compaction methods. *J. Build. Eng.* **2023**, *77*, 107430. [[CrossRef](#)]
10. Chen, T.; Luan, Y.; Ma, T.; Zhu, J.; Ma, S. Mechanical and microstructural characteristics of different interfaces in cold recycled mixture containing cement and asphalt emulsion. *J. Clean. Prod.* **2020**, *258*, 120674. [[CrossRef](#)]
11. Gao, L.; Ni, F.; Luo, H.; Charmot, S. Characterization of air voids in cold in-place recycling mixtures using X-ray computed tomography. *Constr. Build. Mater.* **2015**, *84*, 429–436. [[CrossRef](#)]
12. Kim, Y.; Lee, H.D. Performance evaluation of Cold In-Place Recycling mixtures using emulsified asphalt based on dynamic modulus, flow number, flow time, and raveling loss. *KSCE J. Civ. Eng.* **2012**, *16*, 586–593. [[CrossRef](#)]
13. Jiang, J.; Ni, F.; Zheng, J.; Han, Y.; Zhao, X. Improving the high-temperature performance of cold recycled mixtures by polymer-modified asphalt emulsion. *J. Pavement Eng.* **2018**, *21*, 41–48. [[CrossRef](#)]
14. Zhang, J.; Zheng, M.; Pei, J.; Zhang, J.; Li, R. Research on low temperature performance of emulsified asphalt cold recycled mixture and improvement measures based on fracture energy. *Materials* **2020**, *13*, 3176. [[CrossRef](#)] [[PubMed](#)]
15. Yan, J.; Leng, Z.; Li, F.; Zhu, H.; Bao, S. Early-age strength and long-term performance of asphalt emulsion cold recycled mixes with various cement contents. *Constr. Build. Mater.* **2017**, *137*, 153–159. [[CrossRef](#)]
16. Yang, Y.; Yang, Y.; Qian, B. Performance and microstructure of cold recycled mixes using asphalt emulsion with different contents of cement. *Materials* **2019**, *12*, 2548. [[CrossRef](#)] [[PubMed](#)]
17. Dong, S.; Wang, D.; Hao, P.; Zhang, Q.; Bi, J.; Chen, W. Quantitative assessment and mechanism analysis of modification approaches for cold recycled mixtures with asphalt emulsion. *J. Clean. Prod.* **2021**, *323*, 129163. [[CrossRef](#)]
18. Du, S. Effect of different fibres on the performance properties of cold recycled mixture with asphalt emulsion. *J. Pavement Eng.* **2021**, *23*, 1–10. [[CrossRef](#)]
19. Xu, S.; Ruan, P.; Lu, Z.; Liang, L.; Han, B.; Hong, B. Effects of the high temperature and heavy load on the rutting resistance of cold-mix emulsified asphalt mixture. *Constr. Build. Mater.* **2021**, *298*, 123831. [[CrossRef](#)]
20. Azadgoleh, M.A.; Modarres, A.; Ayar, P. Effect of polymer modified bitumen emulsion production method on the durability of recycled asphalt mixture in the presence of deicing agents. *Constr. Build. Mater.* **2021**, *307*, 124958. [[CrossRef](#)]
21. Yang, Y.; Yue, L.; Cui, H.; Yang, Y. Simulation and evaluation of fatigue damage of cold recycled mixtures with bitumen emulsion. *Constr. Build. Mater.* **2023**, *364*, 129976. [[CrossRef](#)]

22. Lin, J.; Hong, J.; Xiao, Y. Dynamic characteristics of 100% cold recycled asphalt mixture using asphalt emulsion and cement. *J. Clean. Prod.* **2017**, *156*, 337–344. [[CrossRef](#)]
23. Guo, W.; Guo, X.; Chen, W.; Li, Y.; Sun, M.; Dai, M. Laboratory assessment of deteriorating performance of nano hydrophobic silane silica modified asphalt in spring-thaw season. *Appl. Sci.* **2019**, *9*, 2305. [[CrossRef](#)]
24. Yang, Y.; Sun, Z.; Yang, Y.; Yue, L.; Chen, G. Effects of freeze–thaw cycles on performance and microstructure of cold recycled mixtures with asphalt emulsion. *Coatings* **2022**, *12*, 802. [[CrossRef](#)]
25. Lachance-Tremblay, E.; Perraton, D.; Vaillancourt, M.; Benedetto, H. Effect of hydrated lime on linear viscoelastic properties of asphalt mixtures with glass aggregates subjected to freeze–thaw cycles. *Constr. Build. Mater.* **2018**, *184*, 58–67. [[CrossRef](#)]
26. You, L.; You, Z.; Dai, Q.; Guo, S.; Wang, J.; Schultz, M. Characteristics of water-foamed asphalt mixture under multiple freeze-thaw cycles, Laboratory evaluation. *J. Mater. Civ. Eng.* **2018**, *30*, 04018270. [[CrossRef](#)]
27. Fan, Z.; Xu, H.; Xiao, J.; Tan, Y. Effects of freeze-thaw cycles on fatigue performance of asphalt mixture and development of fatigue-freeze-thaw (FFT) uniform equation. *Constr. Build. Mater.* **2020**, *242*, 118043. [[CrossRef](#)]
28. Fu, L.; Zhou, H.; Yuan, P.; An, W.; Chen, X. Damage fracture characterization of asphalt mixtures considering freeze-thaw cycling and aging effects based on acoustic emission monitoring. *Materials* **2021**, *14*, 5930. [[CrossRef](#)]
29. Wang, T.; Chen, Y.; Zhu, C.; Liu, H.; Ma, C.; Wang, X.; Qu, T. High- and low-temperature fracture behavior of pervious asphalt mixtures under different freeze–thaw cycles based on acoustic emission technique. *Arab. J. Geosci.* **2022**, *15*, 1542. [[CrossRef](#)]
30. Ud Din, I.M.; Mir, M.S.; Farooq, M.A. Effect of freeze-thaw cycles on the properties of asphalt pavements in cold regions: A Review. *Transp. Res. Procedia* **2020**, *48*, 3634–3641. [[CrossRef](#)]
31. Xu, H.; Guo, W.; Tan, Y. Internal structure evolution of asphalt mixtures during freeze-thaw cycles. *Mater. Des.* **2015**, *86*, 436–446. [[CrossRef](#)]
32. Xu, H.; Shi, H.; Zhang, H.; Li, H.; Leng, Z.; Tan, Y. Evolution of dynamic flow behavior in asphalt mixtures exposed to freeze-thaw cycles. *Constr. Build. Mater.* **2020**, *255*, 119320. [[CrossRef](#)]
33. Wang, J.; Yu, X.; Ding, G.; Si, J.; Xing, M.; Xie, R. Strength and toughness attenuation mechanism of biobased cold-mixed epoxy asphalt under freeze–thaw cycles. *Int. J. Pavement Eng.* **2022**, 1–9. [[CrossRef](#)]
34. Jin, D.; Yin, L.; Xin, K.; You, Z. Comparison of asphalt emulsion-based chip seal and hot rubber asphalt-based chip seal. *Case Stud. Constr. Mater.* **2023**, *18*, e02175. [[CrossRef](#)]
35. Zhao, H.; Ren, J.; Chen, Z.; Luan, H.; Yi, J. Freeze and thaw field investigation of foamed asphalt cold recycling mixture in cold region. *Case Stud. Constr. Mater.* **2021**, *15*, e00710. [[CrossRef](#)]
36. Löfqvist, L.; Balieu, R.; Kringos, N. Multiscale model for predicting freeze-thaw damage in asphalt mixtures. *Int. J. Pavement Eng.* **2022**, *23*, 5048–5065. [[CrossRef](#)]
37. Cheng, Y.; Yu, D.; Tan, G.; Zhu, C. Low-temperature performance and damage constitutive model of eco-friendly basalt fiber–diatomite-modified asphalt mixture under freeze–thaw cycles. *Materials* **2018**, *11*, 2148. [[CrossRef](#)]
38. Yang, Y.; Cui, H.; Yang, Y.; Zhang, H.; Liu, H. Effect of freeze-thaw cycle on performance of unsaturated emulsified asphalt cold recycled mixture. *J. Jilin Univ. Eng. Technol. Ed.* **2022**, *52*, 2352–2359. [[CrossRef](#)]
39. Yang, Y.; Wang, H.; Yang, Y. Characterization of air voids in cold recycled mixtures with emulsified asphalt under freeze-thaw cycles. *Mater. Rev.* **2022**, *36*, 69–75.
40. *JTG T5521-2019*; Technical Specifications for Highway Asphalt Pavement Recycling. China Communications Press: Beijing, China, 2019.
41. *JTG F40-2004*; Technical Specifications for Construction of Highway Asphalt Pavements. China Communications Press: Beijing, China, 2004.
42. *JTG E40-2007*; Test Methods of Soils for Highway Engineering. China Communications Press: Beijing, China, 2007.
43. Duojie, C.; Si, W.; Ma, B.; Hu, Y.; Xue, L.; Wang, X. Assessment of freeze-thaw cycles impact on flexural tensile characteristics of asphalt mixture in cold regions. *Math. Probl. Eng.* **2021**, *2021*, 6697693. [[CrossRef](#)]
44. *JTG D50-2017*; Specifications for Design of Highway Asphalt Pavement. China Communications Press: Beijing, China, 2017.
45. *JTG E20-2011*; Standard Test Methods of Bitumen and Bituminous Mixtures for Highway Engineering. China Communications Press: Beijing, China, 2011.
46. Tan, Y.; Zhao, L.; Lan, B.; Liang, M. Research on freeze-thaw damage model and life prediction of asphalt mixture. *J. Highw. Transp. Res. Dev.* **2011**, *28*, 1–7.
47. Chen, Y.; Yu, D.; Tan, G.; Wang, W.; Zhang, P. Evolution on freeze-thaw damage of basalt fiber asphalt mixture. *J. Harbin Eng. Univ.* **2019**, *40*, 518–524.

**Disclaimer/Publisher’s Note:** The statements, opinions and data contained in all publications are solely those of the individual author(s) and contributor(s) and not of MDPI and/or the editor(s). MDPI and/or the editor(s) disclaim responsibility for any injury to people or property resulting from any ideas, methods, instructions or products referred to in the content.